DESY 01-039
hep-ph/0104044
April 2001

ISSN 0418-9833

J/ψ plus dijet associated production in two-photon collisions

M. Klasen, B.A. Kniehl, L. Mihaila, M. Steinhauser
II. Institut für Theoretische Physik, Universität Hamburg,
Luruper Chaussee 149, 22761 Hamburg, Germany

arXiv:hep-ph/0104044 v2 18 Jul 2001

Abstract

We study the production of a J/ψ meson in association with one or two jets in $\gamma\gamma$ collisions concentrating on the direct-photon contribution, which is expected to be dominant for large J/ψ-meson transverse momentum and/or large dijet invariant mass. We work at leading order in the factorization formalism of nonrelativistic QCD and include all relevant colour-octet processes. We present distributions in J/ψ-meson transverse momentum and rapidity appropriate for CERN LEP2, a future e^+e^- linear collider, and a possible $\gamma\gamma$ collider mode of the latter. In the case of the e^+e^- linear collider, we assume the beamstrahlung spectrum appropriate for DESY TESLA.

PACS numbers: 12.38.Bx, 13.65.+i, 14.40.Gx

1 Introduction

Since its discovery in 1974, the J/ψ meson has provided a useful laboratory for quantitative tests of quantum chromodynamics (QCD) and, in particular, of the interplay of perturbative and nonperturbative phenomena. The factorization formalism of nonrelativistic QCD (NRQCD) [1] provides a rigorous theoretical framework for the description of heavy-quarkonium production and decay. This formalism implies a separation of short-distance coefficients, which can be calculated perturbatively as expansions in the strong-coupling constant α_s, from long-distance matrix elements (MEs), which must be extracted from experiment. The relative importance of the latter can be estimated by means of velocity scaling rules, i.e. the MEs are predicted to scale with a definite power of the heavy-quark (Q) velocity v in the limit $v \ll 1$. In this way, the theoretical predictions are organized as double expansions in α_s and v. A crucial feature of this formalism is that it takes into account the complete structure of the $Q\overline{Q}$ Fock space, which is spanned by the states ${}^{2S+1}L_J^{(a)}$ with definite spin S, orbital angular momentum L, total angular momentum J, and colour multiplicity $a = \underline{1}, \underline{8}$. In particular, this formalism predicts the existence of colour-octet processes in nature. This means that $Q\overline{Q}$ pairs are produced at short distances in colour-octet states and subsequently evolve into physical (colour-singlet) quarkonia by the nonperturbative emission of soft gluons. In the limit $v \to 0$, the traditional colour-singlet model (CSM) [2,3] is recovered. The greatest triumph of this formalism was that it was able to correctly describe [4,5] the cross section of inclusive charmonium hadroproduction measured in $p\overline{p}$ collisions at the Fermilab Tevatron [6], which had turned out to be more than one order of magnitude in excess of the theoretical prediction based on the CSM.

In order to convincingly establish the phenomenological significance of the colour-octet processes, it is indispensable to identify them in other kinds of high-energy experiments as well. Studies of charmonium production in ep photoproduction, ep and νN deep-inelastic scattering, e^+e^- annihilation, $\gamma\gamma$ collisions, and b-hadron decays may be found in the literature; see Ref. [7] and references cited therein. Furthermore, the polarization of charmonium, which also provides a sensitive probe of colour-octet processes, was investigated [8,9,10,11]. None of these studies was able to prove or disprove the NRQCD factorization hypothesis. On the one hand, the theoretical predictions to be compared with existing experimental data are, apart from very few exceptions [12,13,14], of lowest order (LO) and thus suffer from considerable uncertainties, mostly from the dependences on the renormalization and factorization scales and from the lack of information on the nonperturbative MEs. On the other hand, the experimental errors are still rather sizeable. The latter will be dramatically reduced with the upgrades of DESY HERA and the Fermilab Tevatron and with the advent of CERN LHC and hopefully a future e^+e^- linear collider (LC) such as DESY TESLA. On the theoretical side, it is necessary to calculate the next-to-leading-order (NLO) corrections to the hard-scattering cross sections and to include the effective operators which are suppressed by higher powers in v.

In this paper, we take a first step towards the complete NLO analysis of a $2 \to 2$ process of heavy-quarkonium production in the NRQCD factorization formalism. We consider the

inclusive production of J/ψ mesons in $\gamma\gamma$ collisions, $\gamma\gamma \to J/\psi + X$, where X denotes the hadronic remnant. The photons can originate from hard initial-state bremsstrahlung in e^+e^- annihilation. At high-energy e^+e^- LCs, an additional source of hard photons is provided by beamstrahlung, the synchrotron radiation emitted by one of the colliding bunches in the field of the opposite bunch. The highest possible photon energies with large enough luminosity may be achieved by converting the e^+e^- LC into a $\gamma\gamma$ collider via back-scattering of high-energetic laser light off the electron and positron beams.

The photons can interact either directly with the quarks participating in the hard-scattering process (direct photoproduction) or via their quark and gluon content (resolved photoproduction). Thus, the process $\gamma\gamma \to J/\psi + X$ receives contributions from the direct, single-resolved, and double-resolved channels. All three contributions are formally of the same order in the perturbative expansion. This may be understood by observing that the parton density functions (PDFs) of the photon have a leading behaviour proportional to $\alpha \ln(M^2/\Lambda_{\mathrm{QCD}}^2) \propto \alpha/\alpha_s$, where α is the fine-structure constant, M is the factorization scale, and Λ_{QCD} is the asymptotic scale parameter of QCD. However, the direct channel is expected to be dominant at large J/ψ-meson transverse momentum (p_T) and/or large invariant mass of the system X. In the following, we focus our attention on the direct channel.

Let us consider the relevant partonic subprocesses that lead to a J/ψ meson with finite p_T, i.e. we leave aside $2 \to 1$ processes. The leading colour-singlet ME of the J/ψ meson is $\left\langle \mathcal{O}_1^{J/\psi}\left({}^3S_1\right)\right\rangle$, its leading colour-octet ones are $\left\langle \mathcal{O}_8^{J/\psi}\left({}^3S_1\right)\right\rangle$, $\left\langle \mathcal{O}_8^{J/\psi}\left({}^1S_0\right)\right\rangle$, and $\left\langle \mathcal{O}_8^{J/\psi}\left({}^3P_J\right)\right\rangle$, with $J = 0, 1, 2$. If we restrict ourselves to purely hadronic final states, then the leading $2 \to 2$ process is $\gamma\gamma \to c\bar{c}\left({}^3S_1^{(8)}\right) g$ [15,16,17]. The relevant Feynman diagrams are depicted in Fig. 1(a). A colour-singlet process is only possible if the system produced together with the $c\bar{c}$ pair forms a colour singlet, too. Among the $2 \to 2$ processes, the leading such process is $\gamma\gamma \to c\bar{c}\left({}^3S_1^{(1)}\right)\gamma$ [15,16,17], which proceeds through the Feynman diagrams shown in Fig. 1(b). The leading $2 \to 3$ processes are $\gamma\gamma \to c\bar{c}(n)gg$ and $\gamma\gamma \to c\bar{c}(n)q\bar{q}$, where $n = {}^3S_1^{(8)}$, ${}^1S_0^{(8)}$, and ${}^3P_J^{(8)}$. The corresponding Feynman diagrams are presented in Figs. 2(a) and 3, respectively. From the technical point of view, it is convenient to evaluate the gluon polarization sum as $\sum_{\mathrm{pol}} \varepsilon_\mu(q)\varepsilon_\nu^*(q) = -g_{\mu\nu}$, at the expense of allowing for Faddeev-Popov ghosts of the gluon to appear in the final state; see Fig. 2(b). The corresponding colour-singlet processes with $n = {}^3S_1^{(1)}$ are forbidden. If there is a gg system in the final state, this follows from Furry's theorem [18] by observing that the ${}^3S_1^{(1)}$ projector effectively closes the c-quark line and acts like a vector coupling and that the two gluons are then in a colour-singlet state, so that we are dealing with a closed fermion loop containing five vector couplings. This was also verified by explicit calculation. In the case of a $c\bar{c}q\bar{q}$ final state, the two quark lines are, at the order considered, connected by a single gluon, which ensures that the $c\bar{c}$ and $q\bar{q}$ pairs are both in a colour-octet state.

In this work, we calculate for the first time the partonic cross sections of these $2 \to 3$ subprocesses. Requiring the two massless partons accompanying the $c\bar{c}$ pair to be hard and isolated, these results can be used to describe experimental data of $\gamma\gamma \to J/\psi + 2j$ if the J/ψ transverse momentum and/or the dijet invariant mass are sufficiently large, so

that the corresponding single- and double-resolved contributions can be neglected. Such data were taken at CERN LEP2 with moderate statistics, but a future e^+e^- collider is bound to deliver a copious amount. This avenue is taken here. As a by-product of our analysis, we check previous results for the $2 \to 2$ processes mentioned above [15,16,17]. In addition, we present the cross section of the partonic subprocess $\gamma\gamma \to c\bar{c}\left({}^1P_1^{(8)}\right) g$. Since $\left\langle \mathcal{O}_8^{J/\psi}\left({}^1P_1\right)\right\rangle$, which has not yet been extracted from experimental data, is formally of $O(v^4)$ relative to $\left\langle \mathcal{O}_8^{J/\psi}\left({}^3S_1\right)\right\rangle$, this yields a relativistic correction to the cross section of $\gamma\gamma \to J/\psi + j$.

On the other hand, the $2 \to 3$ cross sections under consideration here constitute an essential ingredient for the calculation of the NLO corrections to the inclusive cross section of $\gamma\gamma \to J/\psi + X$. In fact, integrating out the phase space of the two massless partons, one obtains the real radiative corrections, which suffer from both infrared (IR) singularities and collinear ones associated with the incoming photon legs. The latter are factorized, at some factorization scale M, and absorbed into the bare photon PDFs appearing in the appropriate single- and double-resolved cross sections, so as to render these bare PDFs renormalized. In this way, the direct, single-resolved, and double-resolved cross sections all become M dependent. However, this M dependence cancels in their sum, up to terms beyond NLO. The IR singularities cancel when the real radiative corrections are combined with the virtual ones. Finally, the ultraviolet (UV) radiative corrections contained in the latter are removed by renormalizing the couplings, masses, wave-functions, and non-perturbative MEs appearing in the LO cross section of $\gamma\gamma \to J/\psi + X$.

The single- and double-resolved cross sections of $\gamma\gamma \to J/\psi + j$ were studied in Refs. [16,17], on the basis of the analytic results of Refs. [2,9,19] and [3,5,9], respectively, and found to be generally more important than the direct one, especially for small values of p_T. For the reasons explained above, our analysis is complementary to the ones of Refs. [16,17].

This paper is organized as follows. In Section 2, we present, in analytic form, the cross sections of the partonic subprocesses $\gamma\gamma \to c\bar{c}\left({}^3S_1^{(8)}\right) g$, $\gamma\gamma \to c\bar{c}\left({}^3S_1^{(1)}\right)\gamma$, and $\gamma\gamma \to c\bar{c}\left({}^1P_1^{(8)}\right) g$. Furthermore, we describe the kinematics of the $2 \to 2$ and $2 \to 3$ processes. The analytic results for the latter are too long to be listed. In Section 3, we present our numerical results for the cross sections of $\gamma\gamma \to J/\psi + X$, where $X = j, \gamma$, and $\gamma\gamma \to J/\psi + 2j$ appropriate for LEP2, TESLA, and the $\gamma\gamma$ collider mode of the latter. Our conclusions are summarized in Section 4.

2 Details of the calculation

To start with, we list the cross sections of the partonic subprocesses $\gamma\gamma \to c\bar{c}\left({}^3S_1^{(8)}\right) g$, $\gamma\gamma \to c\bar{c}\left({}^3S_1^{(1)}\right)\gamma$, and $\gamma\gamma \to c\bar{c}\left({}^1P_1^{(8)}\right) g$. Except for the last case, which we only consider at LO, we work in dimensional regularization with $D = 4 - 2\epsilon$ space-time dimension and introduce a 't Hooft mass μ. In this way, our results can be employed for a future NLO analysis as they stand. In the LO evaluation to be performed in Section 3, we put $\epsilon = 0$.

We apply the projection method of Ref. [13], which is equivalent to the D-dimensional matching procedure of Ref. [20], in order to extract the short-distance coefficients which multiply the MEs. However, in order to conform with common standards, we adopt the normalizations of the MEs from Ref. [1] rather than from Ref. [13]. We find

$$\begin{aligned}\frac{d\sigma}{dt}\left(\gamma\gamma \to c\bar{c}\left({}^3S_1^{(8)}\right) g\right) &= \frac{1}{4(1-\epsilon)^2}\frac{1}{\Gamma(1-\epsilon)}\left(\frac{4\pi\mu^2 s}{tu}\right)^{\epsilon}\frac{1}{16\pi s^2}(4\pi)^3 2N_c C_F \alpha_s Q_c^4 \alpha^2 M \\ &\times \frac{\left\langle \mathcal{O}_8^{J/\psi}\left({}^3S_1\right)\right\rangle}{n_g}\frac{256}{3-2\epsilon} \\ &\times \frac{(2-5\epsilon)stu(s+t+u)+2(1-\epsilon)^2(s^2t^2+s^2u^2+t^2u^2)}{(s+t)^2(s+u)^2(t+u)^2}, \quad (1)\end{aligned}$$

where $Q_c = 2/3$ and $M/2 = m_c$ are the fractional electric charge and the mass of the charm quark, respectively, s, t, and u are the Mandelstam variables, the first prefactor stems from the average over the photon polarization, $N_c = 3$, $C_F = (N_c^2-1)/(2N_c)$, and $n_g = N_c^2 - 1$. The expression for $d\sigma/dt\left(\gamma\gamma \to c\bar{c}\left({}^3S_1^{(1)}\right)\gamma\right)$ emerges from Eq. (1) through the substitution [15]

$$2N_c C_F \alpha_s \frac{\left\langle \mathcal{O}_8^{J/\psi}\left({}^3S_1\right)\right\rangle}{n_g} \to Q_c^2 \alpha \left\langle \mathcal{O}_1^{J/\psi}\left({}^3S_1\right)\right\rangle, \quad (2)$$

in contrast to what is stated in Ref. [16]. In the physical limit, $\epsilon = 0$, Eq. (1) agrees with Eq. (7) of Ref. [15], while it disagrees with the corresponding result presented in Ref. [16]. Our result for $d\sigma/dt\left(\gamma\gamma \to c\bar{c}\left({}^3S_1^{(1)}\right)\gamma\right)$ disagrees with Eq. (7) of Ref. [16]. Furthermore, we obtain

$$\begin{aligned}\frac{d\sigma}{dt}\left(\gamma\gamma \to c\bar{c}\left({}^1P_1^{(8)}\right) g\right) &= \frac{1}{4}\frac{1}{16\pi s^2}\frac{(4\pi)^3 2N_c C_F \alpha_s Q_c^4 \alpha^2}{M}\frac{\left\langle \mathcal{O}_8^{J/\psi}\left({}^1P_1\right)\right\rangle}{n_g} \\ &\times \frac{2048}{3[(s+t)^3(s+u)^3(t+u)^3]}\{-7(stu)^2(s+t+u) \\ &- 5stu(s+t+u)^2(st+su+tu)+4stu(s+t+u)^4 \\ &- [s^2t^2(s+t)^3+s^2u^2(s+u)^3+t^2u^2(t+u)^3] \\ &+ st(s+t)^5+su(s+u)^5+tu(t+u)^5\}. \quad (3)\end{aligned}$$

For definiteness, the non-perturbative MEs in Eqs. (1) and (3) refer to the J/ψ meson, but these equations are also valid for other heavy quarkonia.

The respective cross section of $e^+e^- \to e^+e^-J/\psi + X$ is obtained by convoluting the sum of these partonic cross sections with the photon flux functions $f_{\gamma/e}(x)$, where x denotes the fraction of the electron or positron beam energy carried by the bremsstrahlung, beamstrahlung, or laser photons. Working in the e^+e^- centre-of-mass (CM) frame and denoting the nominal e^+e^- energy by $\sqrt{S}$, the transverse momentum and rapidity of the

J/ψ meson by p_T and y, and those of the gluon jet or hard photon by p_{T1} and y_1, we have

$$\frac{d^3\sigma(e^+e^- \to e^+e^- J/\psi + X)}{dp_T^2 dy dy_1} = x_+ f_{\gamma/e}(x_+) x_- f_{\gamma/e}(x_-) \sum_n \sum_{a=g,\gamma} \frac{d\sigma}{dt}(\gamma\gamma \to c\bar{c}(n)a), \quad (4)$$

where $x_\pm = [m_T \exp(\pm y) + p_{T1} \exp(\pm y_1)]/\sqrt{S}$, with $m_T = \sqrt{p_T^2 + M^2}$ and $p_{T1} = p_T$. The Mandelstam variables are then given by $s = x_+ x_- S$, $t = M^2 - x_+\sqrt{S} m_T \exp(-y)$, and $u = M^2 - x_-\sqrt{S} m_T \exp(y)$. For a given value of $\sqrt{S}$, the accessible phase space is defined by

$$\begin{aligned} & 0 \le p_T \le \frac{S - M^2}{2\sqrt{S}}, \\ & |y| \le \mathrm{Arcosh}\, \frac{S + M^2}{2\sqrt{S} m_T}, \\ & -\ln \frac{\sqrt{S} - m_T \exp(-y)}{p_{T1}} \le y_1 \le \ln \frac{\sqrt{S} - m_T \exp(y)}{p_{T1}}. \end{aligned} \quad (5)$$

We now turn to the case where the system X consists of two hadron jets. Calling the azimuthal angles, transverse momenta, and rapidities of the latter ϕ_i, p_{Ti}, and y_i, with $i = 1, 2$, we have

$$\begin{aligned} \frac{d^6\sigma(e^+e^- \to e^+e^- J/\psi + 2j)}{dp_T^2 dy d\phi_1 dp_{T1}^2 dy_1 dy_2} = & \frac{1}{512\pi^4 s^2} x_+ f_{\gamma/e}(x_+) x_- f_{\gamma/e}(x_-) \\ & \times \sum_n \sum_{ab=gg,q\bar{q}} \overline{|\mathcal{M}^2|}(\gamma\gamma \to c\bar{c}(n)ab), \end{aligned} \quad (6)$$

where $x_\pm = [m_T \exp(\pm y) + p_{T1} \exp(\pm y_1) + p_{T2} \exp(\pm y_2)]/\sqrt{S}$, with $p_{T2} = \sqrt{p_T^2 + p_{T1}^2 + 2 p_T p_{T1} \cos\phi_1}$. The analytic expressions for the various spin-averaged, squared matrix elements $\overline{|\mathcal{M}^2|}(\gamma\gamma \to c\bar{c}(n)ab)$ are too lengthy to be listed here. The accessible phase space is now defined by

$$\begin{aligned} & 0 \le p_T \le \frac{S - M^2}{2\sqrt{S}}, \\ & |y| \le \mathrm{Arcosh}\, \frac{S + M^2}{2\sqrt{S} m_T}, \\ & 0 \le \phi_1 \le 2\pi, \\ & 0 \le p_{T1} \le \frac{S + M^2 - 2\sqrt{S} m_T \cosh y}{2\left(\sqrt{S + m_T^2 - 2\sqrt{S} m_T \cosh y} + p_T \cos\phi_1\right)}, \\ & \left| y_1 - \frac{1}{2} \ln \frac{\sqrt{S} - m_T \exp(y)}{\sqrt{S} - m_T \exp(-y)} \right| \le \mathrm{Arcosh}\, \frac{S + M^2 - 2\sqrt{S} m_T \cosh y - 2 p_T p_{T1} \cos\phi_1}{2 p_{T1} \sqrt{S + m_T^2 - 2\sqrt{S} m_T \cosh y}}, \\ & -\ln \frac{\sqrt{S} - m_T \exp(-y) - p_{T1} \exp(-y_1)}{p_{T2}} \le y_2 \le \ln \frac{\sqrt{S} - m_T \exp(y) - p_{T1} \exp(y_1)}{p_{T2}}. \end{aligned} \quad (7)$$

3 Numerical analysis

We are now in a position to explore the phenomenological implications of our results. We use $\alpha = 1/137.036$ [21] and evaluate $\alpha_s^{(n_f)}(\mu)$ from the LO formula taking the number of active quark flavours to be $n_f = 3$, the renormalization scale to be $\mu = m_T$, and the asymptotic scale parameter to be $\Lambda_{\rm QCD}^{(3)} = 145$ MeV, which corresponds to $\alpha_s^{(5)}(M_Z) = 0.1180$ [22] if the charm- and bottom-quark thresholds are chosen to be at $m_c = 1.5$ GeV and $m_b = 4.5$ GeV [21]. We adopt the nonperturbative J/ψ-meson MEs appropriate for the MRST proton PDFs [23] from Ref. [10], $\left\langle \mathcal{O}_1^{J/\psi}\left({}^3S_1\right)\right\rangle = 1.3$ GeV^3, $\left\langle \mathcal{O}_8^{J/\psi}\left({}^3S_1\right)\right\rangle = 4.4 \times 10^{-3}$ GeV^3, and $M_{3.4}^{J/\psi} = 8.7 \times 10^{-2}$ GeV^3, together with the multiplicity relation

$$\left\langle \mathcal{O}_8^{J/\psi}\left({}^3P_J\right)\right\rangle = (2J+1)\left\langle \mathcal{O}_8^{J/\psi}\left({}^3P_0\right)\right\rangle, \tag{8}$$

which follows from heavy-quark spin symmetry. In want of more specific information, we democratically split the linear combination

$$M_r = \left\langle \mathcal{O}_8^{J/\psi}\left({}^1S_0\right)\right\rangle + \frac{r}{m_c^2}\left\langle \mathcal{O}_8^{J/\psi}\left({}^3P_0\right)\right\rangle \tag{9}$$

as $\left\langle \mathcal{O}_8^{J/\psi}\left({}^1S_0\right)\right\rangle = (r/m_c^2)\left\langle \mathcal{O}_8^{J/\psi}\left({}^3P_0\right)\right\rangle = M_r/2$.

In $\gamma\gamma$ collisions at LEP2, the scattered electrons and positrons are usually antitagged, a typical value for the maximum scattering angle being $\theta_{\rm max} = 33$ mrad [24]. The energy spectrum of the bremsstrahlung photons is then well described in the Weizsäcker-Williams approximation (WWA) [25] by Eq. (27) of Ref. [26]. Values as small as $\theta_{\rm max} = 20$ mrad should be feasible at TESLA [27]. As already mentioned in the Introduction, at high-energy e^+e^- LCs, hard photons also arise from beamstrahlung. The energy spectrum of these beamstrahlung photons is approximately described by Eq. (2.14) of Ref. [28]. It is controlled the beamstrahlung parameter Υ, which is estimated to be $\Upsilon = 0.040$ for TESLA. We coherently superimpose the WWA and beamstrahlung spectra. Finally, in the case of a $\gamma\gamma$ collider, the energy spectrum of the back-scattered laser photons is given by Eq. (6a) of Ref. [29]. It depends on the parameter $\kappa = s_{e\gamma}/m_e^2 - 1$, where $\sqrt{s_{e\gamma}}$ is the CM energy of the charged lepton and the laser photon, and it extends up to $x_{\rm max} = \kappa/(\kappa+1)$, where x is the energy of the back-scattered photons in units of $\sqrt{S}/2$. The optimal value of κ is $\kappa = 2\left(1+\sqrt{2}\right) \approx 4.83$ [30]; for larger values of κ, e^+e^- pairs would be created in the collisions of laser and back-scattered photons. Representative e^+e^- CM energies of LEP2 and TESLA are $\sqrt{S} = 189$ GeV and 500 GeV.

In Figs. 4–8, we quantitatively investigate the cross section of inclusive J/ψ-meson production in the collisions of two bremsstrahlung photons at LEP2. In Figs. 4 and 5, we present for $\gamma\gamma \to J/\psi + X$, where X represents a gluon jet (dot-dashed lines) or a prompt photon (dashed lines), the distributions in transverse momentum p_T and rapidity y of the J/ψ meson, respectively. The solid lines refer to the sum of the contributions for $X = j$ and $X = \gamma$. The cuts on p_T and y are adopted from Ref. [24]. In the case $X = j$, the leading contribution comes from the ${}^3S_1^{(8)}$ channel. The contribution from the

$^1P_1^{(8)}$ channel is suppressed for the reason explained in the Introduction. Furthermore, the value of $\left\langle \mathcal{O}_8^{J/\psi}\left(^1P_1\right)\right\rangle$ is not yet available. Therefore, this contribution is not included in Figs. 4 and 5. The distributions for $X = j$ and $X = \gamma$ only differ by the overall normalization, as is evident from Eq. (2). Obviously, the coupling suppression of the result for $X = \gamma$ is less substantial than the suppression of the result for $X = j$ by the fact that $\left\langle \mathcal{O}_8^{J/\psi}\left(^3S_1\right)\right\rangle$ is of order v^4 relative to $\left\langle \mathcal{O}_1^{J/\psi}\left(^3S_1\right)\right\rangle$. Since we assumed the same experimental set-up for the electron and positron beams, the y distributions displayed in Fig. 5 are all symmetric about $y = 0$. Figure 4 is similar to Fig. 1 of Ref. [17], which we are able to reproduce, adopting the input parameters specified in that reference. We note in passing that Ref. [17], too, disagrees with Ref. [16] for $X = j$ and $X = \gamma$; see the statement contained in Ref. [21] of Ref. [17].

In Figs. 6 and 7, we study the p_T and y distributions of $\gamma\gamma \to J/\psi + jj$, respectively, again imposing the cuts of Ref. [24]. In addition, following Ref. [31], we require for the two jets to have transverse momenta $p_{Ti} > 5$ GeV and rapidities $|y_i| < 2$ $(i = 1, 2)$ and to be separated by $\Delta R = \sqrt{(y_1 - y_2)^2 + (\phi_1 - \phi_2)^2} > 1$ according to the k_T-clustering algorithm [32]. While no actual clustering is performed, the separation of the two jets is necessary to avoid collinear singularities in the final state. In Fig. 6, we analyze the relative importance of the various colour-octet channels. We observe that the $^1S_0^{(8)}$ channel is most important. As is familiar from inclusive J/ψ-meson hadroproduction at the Tevatron [5], the $^1S_0^{(8)}$ and $^3P_J^{(8)}$ channels have very similar p_T dependences for $p_T \gtrsim 5$ GeV. By the same token, this implies that the theoretical uncertainty related to the lack of information on how M_r breaks into $\left\langle \mathcal{O}_8^{J/\psi}\left(^1S_0\right)\right\rangle$ and $\left\langle \mathcal{O}_8^{J/\psi}\left(^3P_0\right)\right\rangle$ is modest. On the other hand, the $^3S_1^{(8)}$-channel contribution falls off less rapidly as p_T increases. The suppression of the $^3S_1^{(8)}$ contribution relative to the combination of the $^1S_0^{(8)}$ and $^3P_J^{(8)}$ ones may be traced to the fact that M_r is almost a factor of 20 larger than $\left\langle \mathcal{O}_8^{J/\psi}\left(^3S_1\right)\right\rangle$ [10]. The total y distribution shown in Fig. 7 (solid line) exhibits a marked minimum at $y = 0$. Its decomposition into the contributions where the dijets are of gg (dotted line) and $q\bar{q}$ (dashed line) origin clarifies that this minimum stems from the latter contribution. This may be understood by observing that the q and $\bar{q}$ quarks may be created from the splitting of the incident photons, in which case they are dominantly collinear to the mother photons. On the other hand, the final-state gluons are either both directly radiated off the heavy-quark line or emerge through the $1 \to 2$ splitting of a virtual gluon that is radiated off the heavy-quark line, so that the resulting y distribution is expected to have a shape similar to the one of $\gamma\gamma \to J/\psi + j$ studied in Fig. 5, which has a maximum at $y = 0$.

In Fig. 8, we make an attempt to obtain a first hint at the size of the NLO correction to the cross section of $\gamma\gamma \to J/\psi + X$, where X is a gluon jet or a prompt photon. To this end, we compare the LO p_T distribution of $\gamma\gamma \to J/\psi + X$ (dotted line), taken from Fig. 4, with the one of $\gamma\gamma \to J/\psi + jj$ after integrating the dijet invariant mass $\sqrt{s_{jj}}$ over all kinematically allowed values with $s_{jj} > M^2$ (lower solid line) and $M^2/20$ (upper solid line). A similar strategy was adopted in Ref. [14] to estimate the NLO correction to J/ψ-meson hadroproduction via the $^3S_1^{(1)}$ channel at finite values of p_T. The dependence on the s_{jj} lower cutoff would be compensated in the full NLO result by the virtual and

soft real corrections, which are not yet available. However, from Fig. 8 we learn that this dependence is reduced as the value of p_T increases. Moreover, the missing part of the NLO contribution should have a similar p_T dependence as the LO result, and it should, therefore, be suppressed relative to the available part, presented in Fig. 8, at large values of p_T. Consequently, we expect the NLO correction factor to be significantly larger than unity in the high-p_T regime. Of course, a solid statement can only be made on the basis of a complete NLO analysis. For comparison, we also indicate in Fig. 8 the ${}^3S_1^{(8)}$-channel portions of the contributions represented by the solid lines. They are scaled down by a factor of 20 to 30, as is naively expected from the $\left\langle \mathcal{O}_8^{J/\psi}\left({}^3S_1\right)\right\rangle$ to M_r ratio [10]. Strictly speaking, $\gamma\gamma \to J/\psi + jj$ contributes to the real QCD correction to $\gamma\gamma \to J/\psi + j$, but not to $\gamma\gamma \to J/\psi + \gamma$. However, the NLO correction to the latter process is suppressed by the factor α/α_s relative to the NLO correction under consideration here, and it can thus be safely neglected.

We now turn to $\gamma\gamma$ collisions at TESLA. As explained above, in the e^+e^- mode, the photons originate from bremsstrahlung and beamstrahlung, while in the $\gamma\gamma$ mode, they arise from the back-scattering of laser light on the incident electron and positron beams. In Figs. 9–12, the contributions due to bremsstrahlung (dashed lines), beamstrahlung (dot-dashed lines), their coherent superposition (solid lines), and Compton scattering (dotted lines) are shown separately. We apply the same cuts on p_T, y, p_{Ti}, and y_i $(i = 1, 2)$ as in the LEP2 case. The p_T and y distributions of $\gamma\gamma \to J/\psi + X$, where it is summed over $X = j$ and $X = \gamma$, are presented in Figs. 9 and 10, respectively. From Eq. (4) we know that small values of p_T typically correspond to small values of x and vice versa. Since the bremsstrahlung and beamstrahlung spectra are peaked at $x = 0$, while the Compton spectrum is peaked at $x = x_{\max}$, it hence follows that the bremsstrahlung and beamstrahlung contributions significantly overshoot the Compton one in the small-p_T regime, while the latter wins out at large values of p_T, a feature which so far has gone unnoticed in the literature. Owing to the rapid fall-off of the p_T distributions in Fig. 9, the corresponding y distributions in Fig. 10 receive their bulk contributions from the small-p_T regime. This explains why the Compton contribution is greatly suppressed relative to the bremsstrahlung and beamstrahlung ones. The beamstrahlung contribution exhibits a prominent peak about $y = 0$ and drops off at $|y| \approx 3$, while the bremsstrahlung one has a flatter shape and dominates for $|y| \gtrsim 2.2$.

The p_T and y distributions of $\gamma\gamma \to J/\psi + jj$, with all the leading colour-octet channels included, are shown in Figs. 11 and 12, respectively. Comparing Fig. 11 with Fig. 9, we observe that now the Compton contribution starts to exceed the one due to bremsstrahlung and beamstrahlung already at $p_T \approx 9$ GeV. This may be understood by observing that it is now possible for x to take large values at small values of p_T if the dijet invariant mass is sufficiently large. As in Fig. 7, the y distributions are symmetric about $y = 0$ and exhibit a local minimum there. This feature is particularly pronounced for the Compton contribution. As in Fig. 10, the beamstrahlung contribution exceeds the bremsstrahlung one in the central y region and only extends out to $|y| \approx 3$, while the bremsstrahlung one dominates for $|y| \gtrsim 2.2$.

4 Conclusions

We calculated the cross section of $\gamma\gamma \to J/\psi + jj$ in direct photoproduction at LO in the NRQCD factorization formalism and provided theoretical predictions for the J/ψ-meson p_T and y distributions in $\gamma\gamma$ collisions via initial-state bremsstrahlung at LEP2 and via bremsstrahlung and beamstrahlung or laser back-scattering at TESLA. We also performed a similar study for $\gamma\gamma \to J/\psi + X$, where X represents a gluon jet or a prompt photon, and compared our results with the literature [15,16,17]. We found agreement with Refs. [15,17], but disagreement with Ref. [16] for both $X = j$ and $X = \gamma$. The contributions due to single-resolved and double-resolved photoproduction are expected to be suppressed if the J/ψ-meson transverse momentum and/or the dijet invariant mass are large as compared to the J/ψ-meson mass. In the CSM, only $\gamma\gamma \to J/\psi + \gamma$ can happen in direct photoproduction. Experimental observation of $\gamma\gamma \to J/\psi + j$ or $\gamma\gamma \to J/\psi + jj$ with the predicted cross sections would provide evidence for the existence of colour-octet processes in nature. An interesting feature of $\gamma\gamma \to J/\psi + jj$ is the appearance of a marked minimum of the y distribution at $y = 0$. The cross section of $\gamma\gamma \to J/\psi + jj$ provides an essential ingredient for the calculation of the NLO correction to the one of $\gamma\gamma \to J/\psi + X$. The virtual and soft real corrections remain to be calculated in order to obtain the full NLO correction factor. Our analysis indicates that the latter is likely to be significantly larger than unity at large values of p_T.

Table 1: Integrated cross sections (in fb) of $\gamma\gamma \to J/\psi + X$, with $X = j, \gamma, jj$, via direct photoproduction in $\gamma\gamma$ collisions at LEP2, TESLA, and its $\gamma\gamma$ option. The applied cuts are $2 < p_T < 12$ GeV and $|y| < 1.5$ for the J/ψ meson and $p_{Ti} > 5$ GeV, $|y_i| < 2$ $(i = 1, 2)$, and $\Delta R > 1$ for the dijet system.

Experiment	$\sigma(J/\psi + j)$	$\sigma(J/\psi + \gamma)$	$\sigma(J/\psi + jj)$
LEP2	4.9	59	0.74
TESLA e^+e^-	22	270	3.5
TESLA $\gamma\gamma$	0.55	6.2	2.4

At e^+e^- colliders, the J/ψ meson can be easily detected through its decay to a $\mu^+\mu^-$ pair, with branching fraction $(5.88 \pm 0.10)\%$ [21]. Unfortunately, the LEP2 experiments have not yet extracted from their recorded data the cross section of inclusive J/ψ-meson production in $\gamma\gamma$ collisions. The OPAL analysis of $\gamma\gamma \to 2j + X$ is based on an integrated luminosity of 384 pb^{-1} [31]. Assuming that the other LEP2 experiments, ALEPH, DELPHI, and L3, have data samples of similar sizes and folding in the $J/\psi \to \mu^+\mu^-$ branching fraction, we conclude that a J/ψ-meson production cross section of 1 pb translates into approximately 90 signal events at LEP2. The design luminosities for the e^+e^- and $\gamma\gamma$ modes of TESLA, with $\sqrt{S} = 500$ GeV, are 3.4×10^{34} cm^{-2}s^{-1} and 0.6×10^{34} cm^{-2}s^{-1} [33], respectively, which corresponds to 340 fb^{-1} and 60 fb^{-1} per year. Thus, a J/ψ-meson

production cross section of 1 fb yields about 20 and 3.5 signal events at TESLA operating in the e^+e^- and $\gamma\gamma$ modes, respectively. In Table 1, we list the integrated cross sections of $\gamma\gamma \to J/\psi + X$, with $X = j, \gamma, jj$, via direct photoproduction in $\gamma\gamma$ collisions at LEP2, TESLA, and its $\gamma\gamma$ option. The applied cuts are $2 < p_T < 12$ GeV and $|y| < 1.5$ for the J/ψ meson and $p_{Ti} > 5$ GeV, $|y_i| < 2$ $(i = 1, 2)$, and $\Delta R > 1$ for the dijet system. The respective numbers of expected signal events emerge through multiplication of the entries in Table 1 with the cross section to event number conversion factors quoted above.

Acknowledgements

We thank J. Lee for a helpful comment on Eq. (2). We are grateful to S. Söldner-Rembold for a useful communication concerning the prospects of measuring the cross section of J/ψ inclusive production in $\gamma\gamma$ collisions at LEP2. This work was supported in part by the Deutsche Forschungsgemeinschaft through Grants No. KL 1266/1-1 and No. KN 365/1-1, by the Bundesministerium für Bildung und Forschung through Grant No. 05 HT9GUA 3, by the European Commission through the Research Training Network *Quantum Chromodynamics and the Deep Structure of Elementary Particles* under Contract No. ERBFMRX-CT98-0194, and by Sun Microsystems through Academic Equipment Grant No. EDUD-7832-000332-GER.

References

[1] G.T. Bodwin, E. Braaten, G.P. Lepage, Phys. Rev. D 51 (1995) 1125; Phys. Rev. D 55 (1997) 5853 (Erratum).

[2] E.L. Berger, D. Jones, Phys. Rev. D 23 (1981) 1521.

[3] R. Baier, R. Rückl, Phys. Lett. 102 B (1981) 364; Z. Phys. C 19 (1983) 251; B. Humpert, Phys. Lett. B 184 (1987) 105; R. Gastmans, W. Troost, T.T. Wu, Phys. Lett. B 184 (1987) 257; Nucl. Phys. B 291 (1987) 731.

[4] E. Braaten, S. Fleming, Phys. Rev. Lett. 74 (1995) 3327; E. Braaten, T.C. Yuan, Phys. Rev. D 52 (1995) 6627.

[5] P. Cho, A.K. Leibovich, Phys. Rev. D 53 (1996) 150; Phys. Rev. 53 (1996) 6203.

[6] CDF Collaboration, F. Abe et al., Phys. Rev. Lett. 69 (1992) 3704; Phys. Rev. Lett. 71 (1993) 2537; Phys. Rev. Lett. 79 (1997) 572; Phys. Rev. Lett. 79 (1997) 578; D0 Collaboration, S. Abachi et al., Phys. Lett. B 370 (1996) 239; D0 Collaboration, B. Abbott et al., Phys. Rev. Lett. 82 (1999) 35.

[7] E. Braaten, S. Fleming, T.C. Yuan, Ann. Rev. Nucl. Part. Sci. 46 (1996) 197; B.A. Kniehl, G. Kramer, Phys. Lett. B 413 (1997) 416.

[8] M. Beneke, M. Krämer, Phys. Rev. D 55 (1997) 5269; A.K. Leibovich, Phys. Rev. D 56 (1997) 4412.

[9] M. Beneke, M. Krämer, M. Vänttinen, Phys. Rev. D 57 (1998) 4258.

[10] E. Braaten, B.A. Kniehl, J. Lee, Phys. Rev. D 62 (2000) 094005; B.A. Kniehl, J. Lee, Phys. Rev. D 62 (2000) 114027.

[11] S. Fleming, A.K. Leibovich, I.Z. Rothstein, Report No. CMU-0005, FERMILAB-Pub-00/321-T, and hep-ph/0012062 (December 2000).

[12] M. Krämer, J. Zunft, J. Steegborn, P.M. Zerwas, Phys. Lett. B 348 (1995) 657; M. Krämer, Nucl. Phys. B 459 (1996) 3.

[13] A. Petrelli, Phys. Lett. B 380 (1996) 159; M.L. Mangano, A. Petrelli, Int. J. Mod. Phys. A 12 (1997) 3887; A. Petrelli, M. Cacciari, M. Greco, F. Maltoni, M.L. Mangano, Nucl. Phys. B 514 (1998) 245; F. Maltoni, M.L. Mangano, A. Petrelli, Nucl. Phys. B 519 (1998) 361.

[14] A. Petrelli, Nucl. Phys. Proc. Suppl. 86 (2000) 533.

[15] J.P. Ma, B.H. McKellar, C.B. Paranavitane, Phys. Rev. D 57 (1998) 606.

[16] G. Japaridze, A. Tkabladze, Phys. Lett. B 433 (1998) 139.

[17] R.M. Godbole, D. Indumathi, M. Krämer, Report No. LC-TH-2001-019, IMSc/2001/01/02, IISc-CTS-01/01, and hep-ph/0101333 (January 2001).

[18] W.H. Furry, Phys. Rev. 51 (1937) 125.

[19] P. Ko, J. Lee, H.S. Song, Phys. Rev. D 54 (1996) 4312; Phys. Rev. D 60 (1999) 119902 (Erratum).

[20] E. Braaten, Y.-Q. Chen, Phys. Rev. D 55 (1997) 2693.

[21] Particle Data Group, D.E. Groom et al., Eur. Phys. J. C 15 (2000) 1.

[22] B.A. Kniehl, G. Kramer, B. Pötter, Phys. Rev. Lett. 85 (2000) 5288.

[23] A.D. Martin, R.G. Roberts, W.J. Stirling, R.S. Thorne, Eur. Phys. J. C 4 (1998) 463.

[24] OPAL Collaboration, G. Abbiendi et al., Eur. Phys. J. C 16 (2000) 579.

[25] E.J. Williams, Proc. Roy. Soc. London A 139 (1933) 163; C.F. v. Weizsäcker, Z. Phys. 88 (1934) 612.

[26] S. Frixione, M.L. Mangano, P. Nason, G. Ridolfi, Phys. Lett. B 319 (1993) 339.

[27] K. Desch, private communication.

[28] P. Chen, T.L. Barklow, M.E. Peskin, Phys. Rev. D 49 (1994) 3209.

[29] I.F. Ginzburg, G.L. Kotkin, V.G. Serbo, V.I. Telnov, Nucl. Instr. Meth. 205 (1983) 47.

[30] V.I. Telnov, Nucl. Instr. Meth. A 294 (1990) 72.

[31] T. Wengler, Report No. hep-ex/0009043, to be published in the proceedings of 30th International Conference on High-Energy Physics (ICHEP 2000), Osaka, Japan, 27 July – 2 August 2000.

[32] S. Catani, Yu.L. Dokshitzer, M.H. Seymour, B.R. Webber, Nucl. Phys. B 406 (1993) 187; S.D. Ellis, D.E. Soper, Phys. Rev. D 48 (1993) 3160.

[33] J. Andruszkow et al., TESLA Technical Design Report, Part II, edited by R. Brinkmann, K. Flöttmann, J. Rossbach, P. Schmüser, N. Walker, H. Weise, Report No. DESY 2001-011, ECFA 2001-209, TESLA Report 2001-23, TESLA-FEL 2001-05 (March 2001), p. 15.

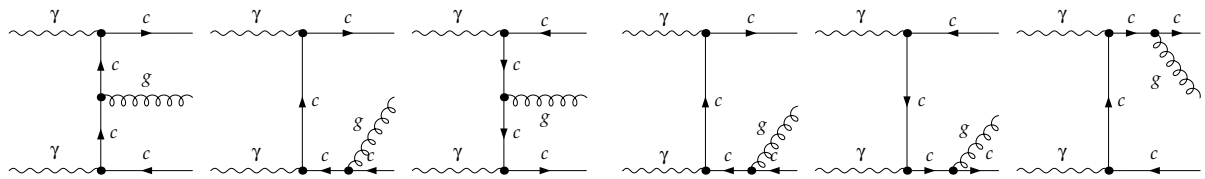

(a)

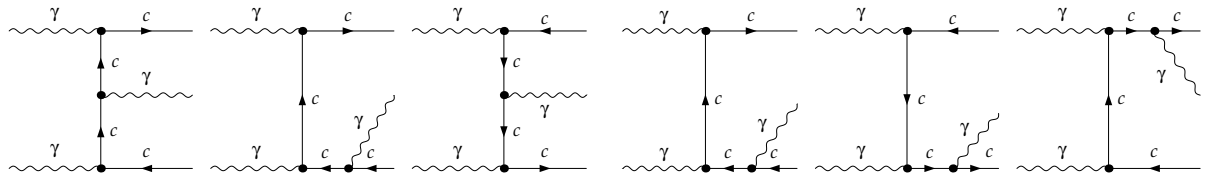

(b)

Figure 1: Feynman diagrams pertinent to the partonic subprocesses (a) $\gamma\gamma \to c\bar{c}g$ and (b) $\gamma\gamma \to c\bar{c}\gamma$.

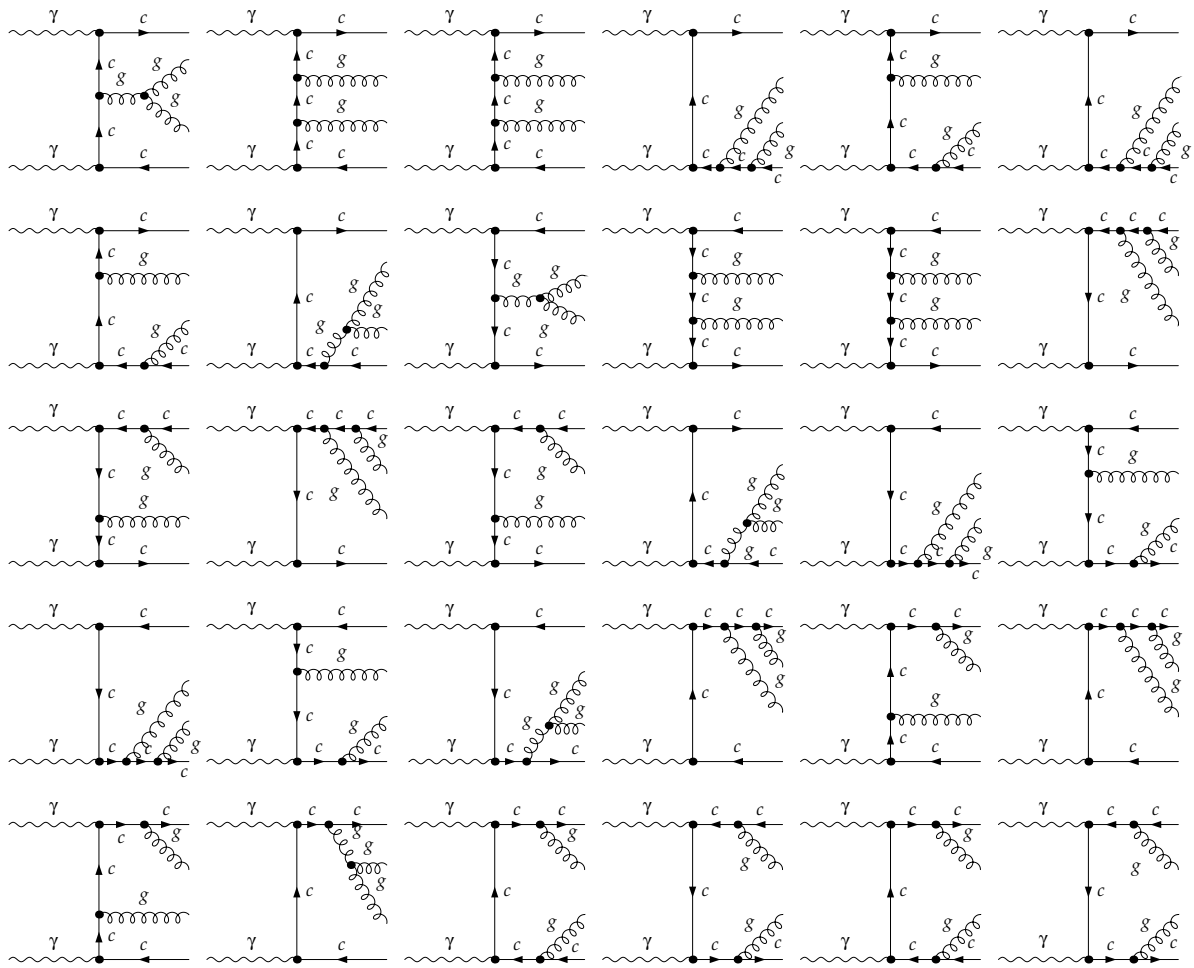

(a)

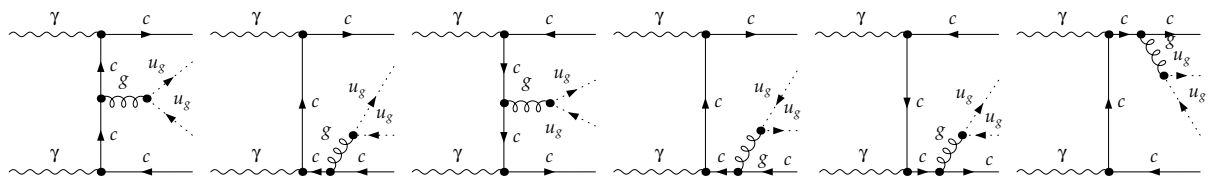

(b)

Figure 2: Feynman diagrams pertinent to the partonic subprocesses (a) $\gamma\gamma \to c\bar{c}gg$ and (b) $\gamma\gamma \to c\bar{c}u_g\bar{u}_g$, where u_g and $\bar{u}_g$ are the Faddeev-Popov ghosts associated with the gluon.

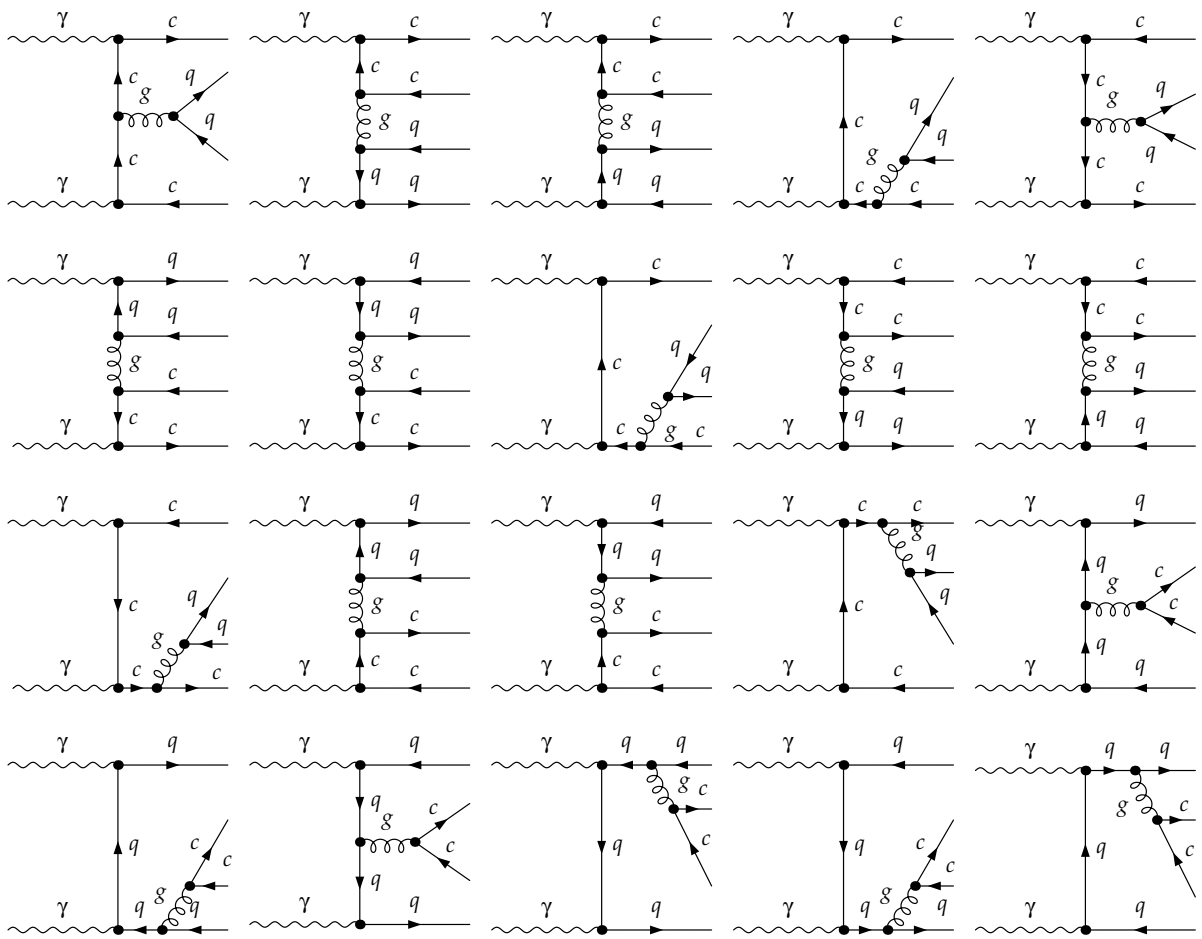

Figure 3: Feynman diagrams pertinent to the partonic subprocess $\gamma\gamma \to c\bar{c}q\bar{q}$, where $q = u, d, s$.

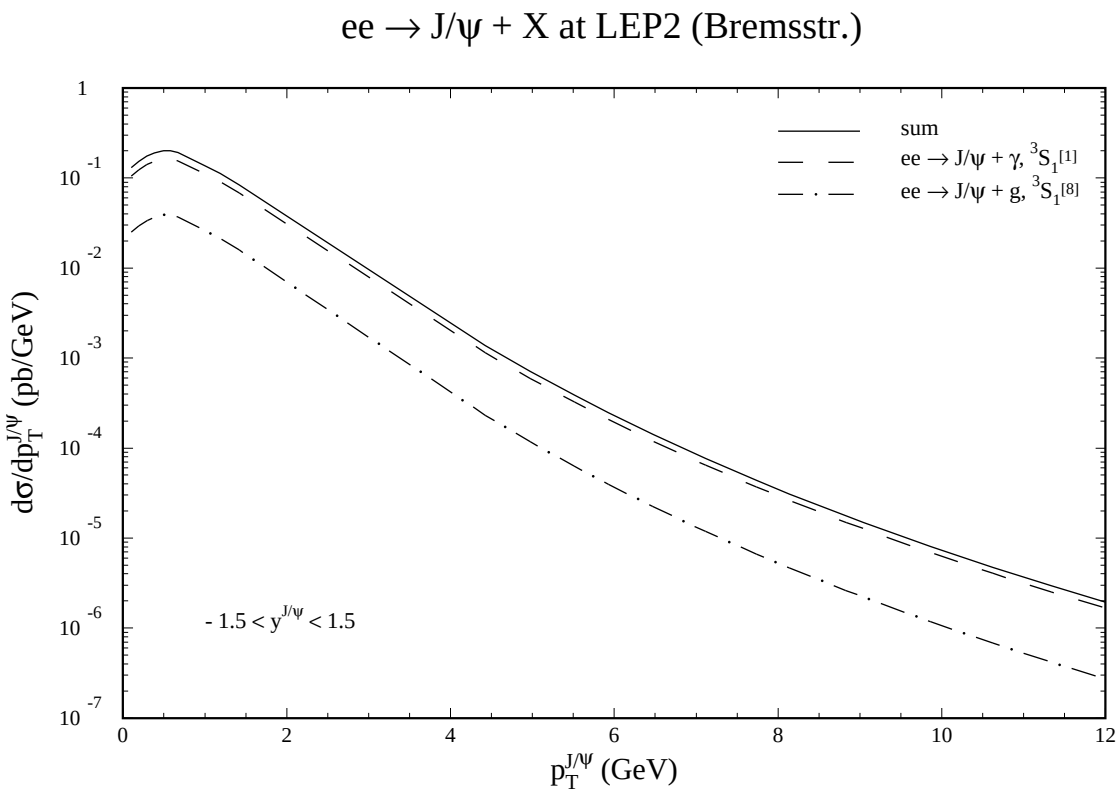

Figure 4: Transverse-momentum distribution $d\sigma/dp_T$, integrated over rapidity interval $|y| < 1.5$, of $\gamma\gamma \to J/\psi + X$, where X represents a gluon jet or a prompt photon, via bremsstrahlung at LEP2. The contributions corresponding to these two final states are also shown separately.

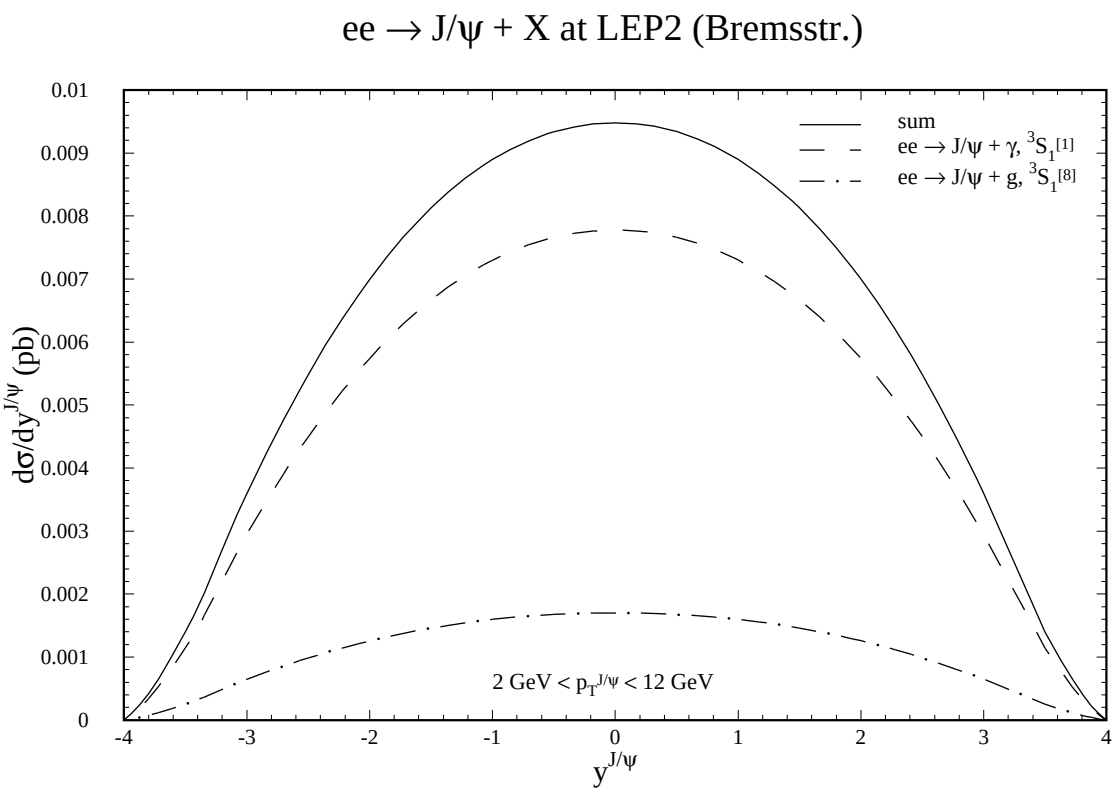

Figure 5: Rapidity distribution $d\sigma/dy$, integrated over transverse-momentum interval $2 < p_T < 12$ GeV, of $\gamma\gamma \to J/\psi + X$, where X represents a gluon jet or a prompt photon, via bremsstrahlung at LEP2. The contributions corresponding to these two final states are also shown separately.

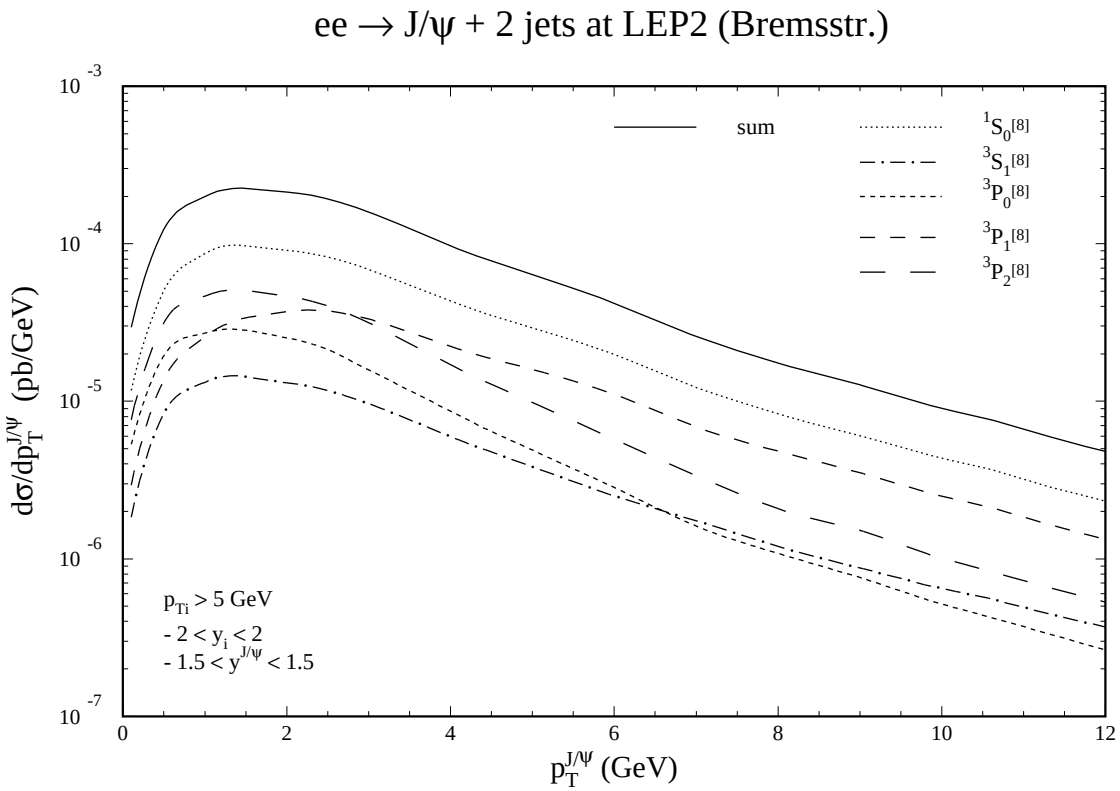

Figure 6: Transverse-momentum distribution $d\sigma/dp_T$ of $\gamma\gamma \to J/\psi + jj$ via bremsstrahlung at LEP2. The contributions due to the various colour-octet channels are also shown separately.

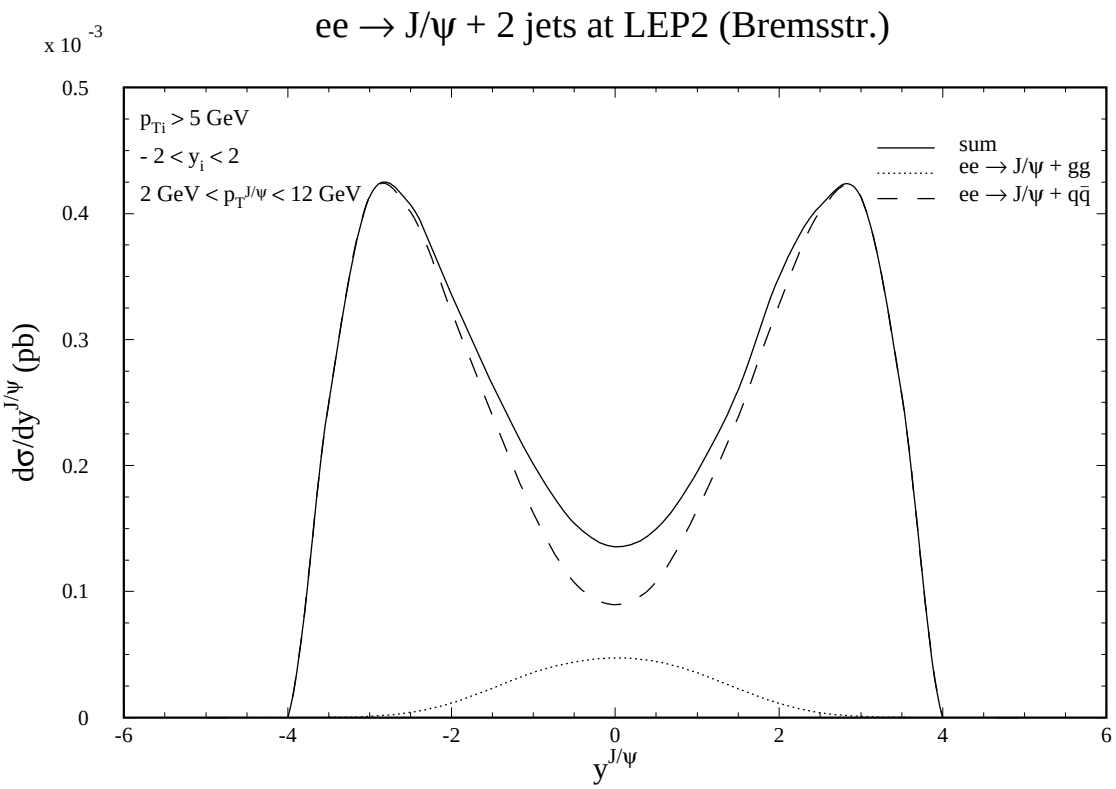

Figure 7: Rapidity distribution $d\sigma/dy$ of $\gamma\gamma \to J/\psi + jj$ via bremsstrahlung at LEP2. The contributions due to quark and gluon dijets are also shown separately.

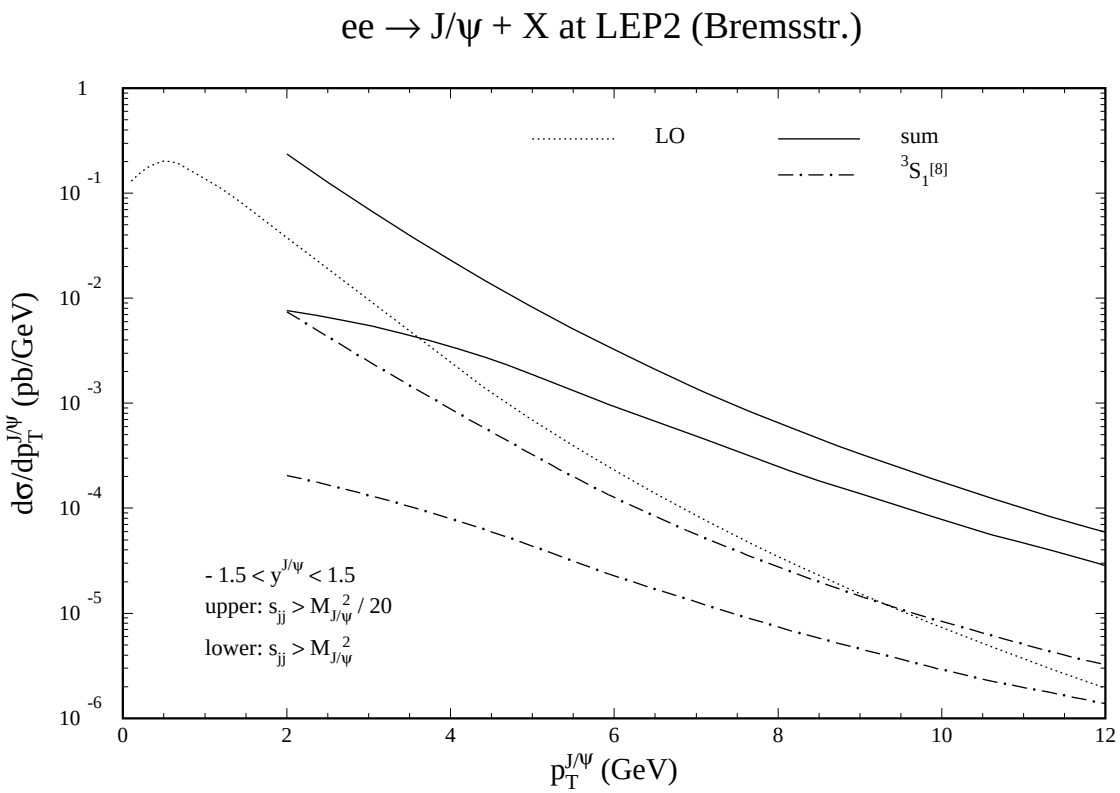

Figure 8: Transverse-momentum distribution $d\sigma/dp_T$ of $\gamma\gamma \to J/\psi + X$ via bremsstrahlung at LEP2. The sum of the LO contributions for $X = j$ and $X = \gamma$ is compared with the $2 \to 3$ part of the NLO contribution for dijet invariant mass $s_{jj} > M^2$ and $M^2/20$. For comparison, also the ${}^3S_1^{(8)}$-channel contributions to the latter are shown.

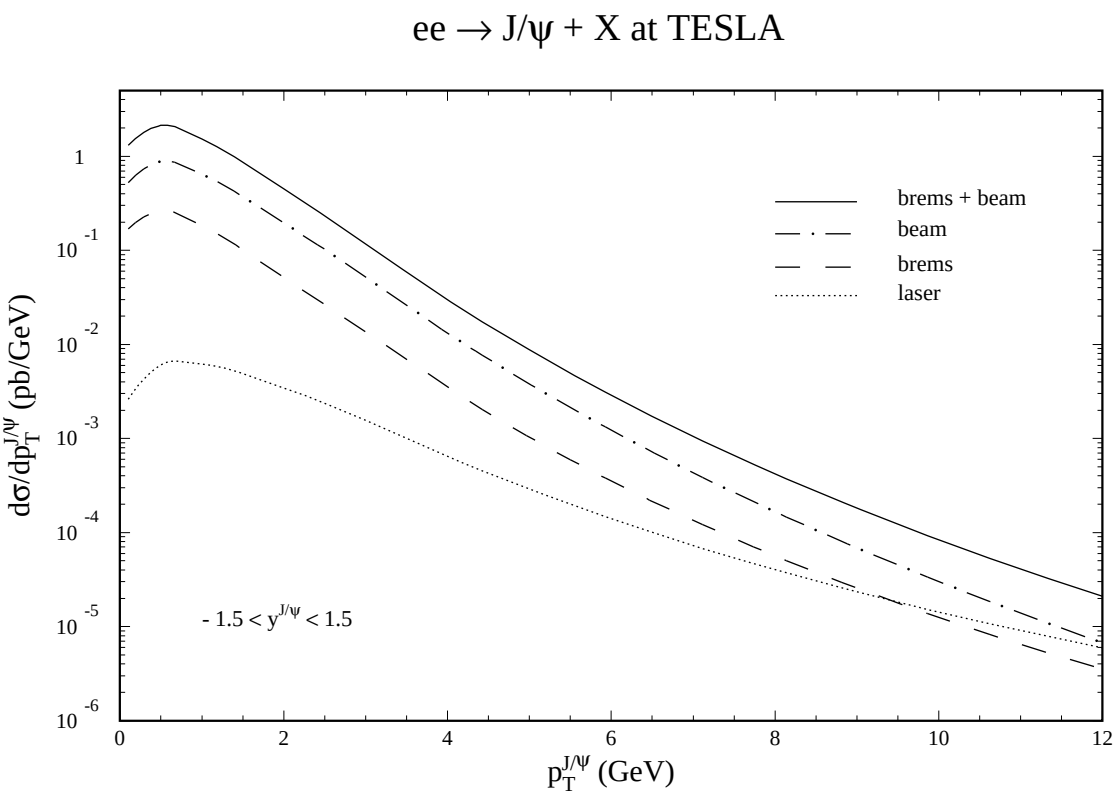

Figure 9: Transverse-momentum distribution $d\sigma/dp_T$, integrated over rapidity interval $|y| < 1.5$, of $\gamma\gamma \to J/\psi + X$, where X represents a gluon jet or a prompt photon, via bremsstrahlung, beamstrahlung, their coherent superposition, and laser back-scattering at TESLA.

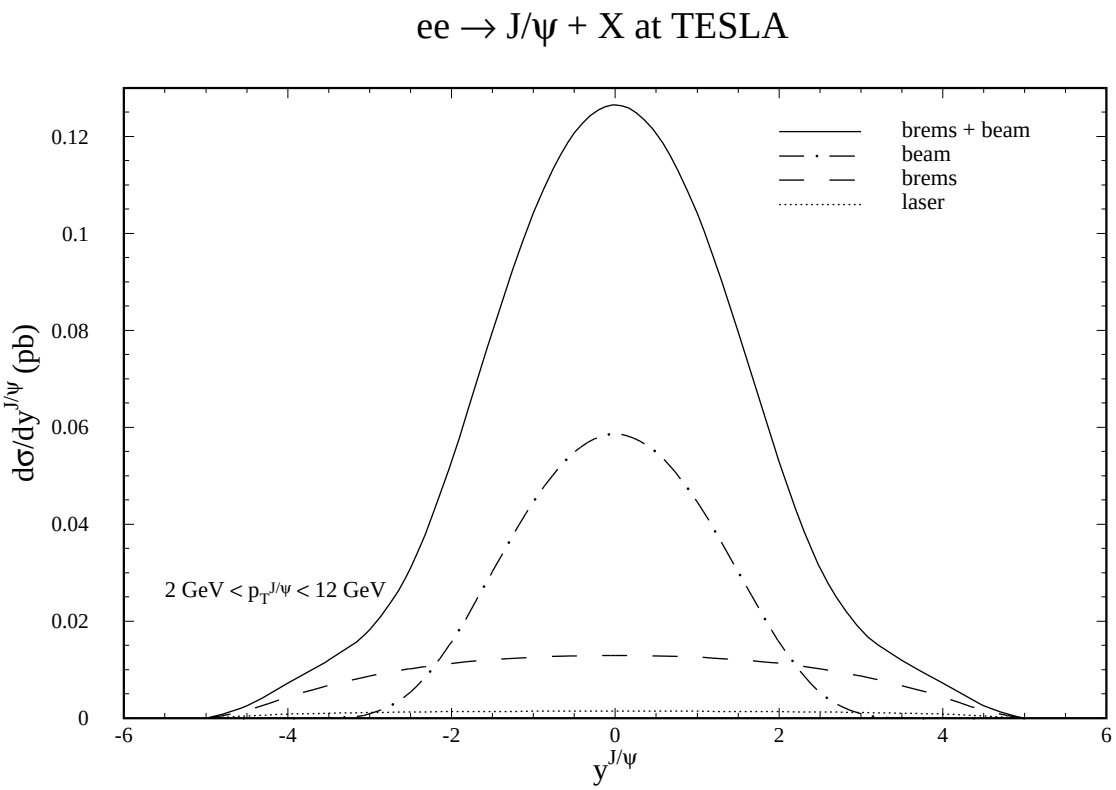

Figure 10: Rapidity distribution $d\sigma/dy$, integrated over transverse-momentum interval $2 < p_T < 12$ GeV, of $\gamma\gamma \to J/\psi + X$, where X represents a gluon jet or a prompt photon, via bremsstrahlung, beamstrahlung, their coherent superposition, and laser backscattering at TESLA.

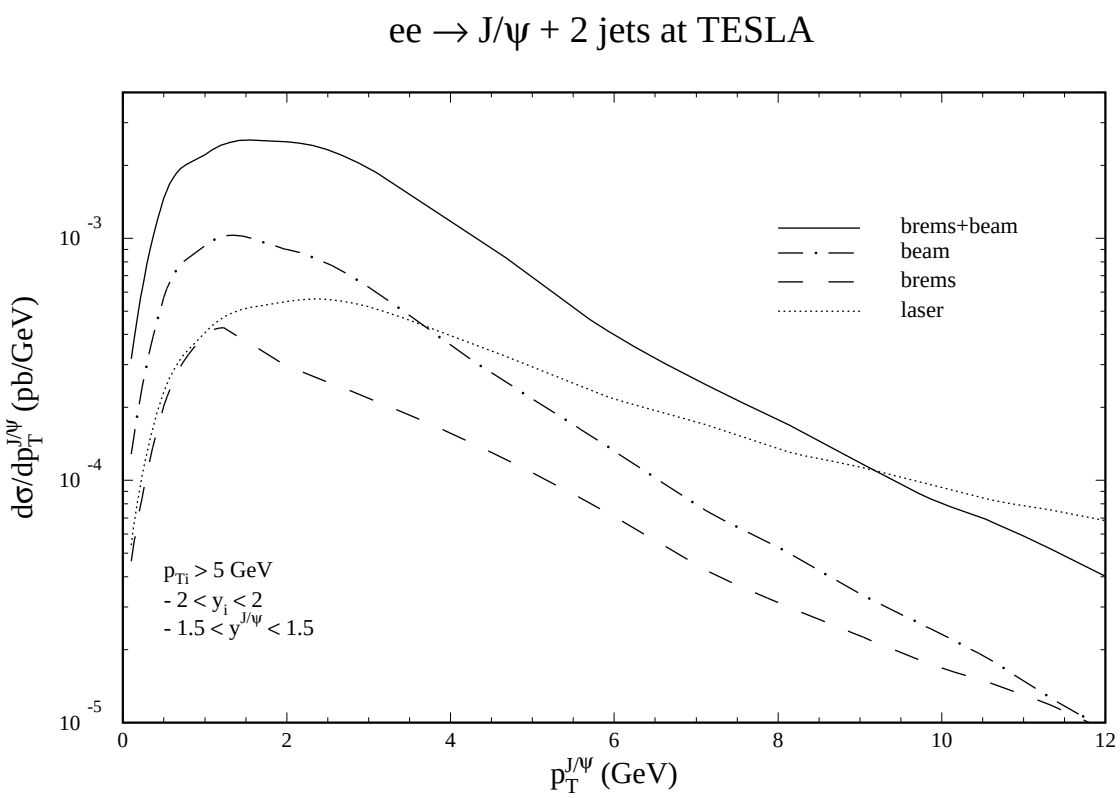

Figure 11: Transverse-momentum distribution $d\sigma/dp_T$ of $\gamma\gamma \to J/\psi + jj$ via bremsstrahlung, beamstrahlung, their coherent superposition, and laser back-scattering at TESLA.

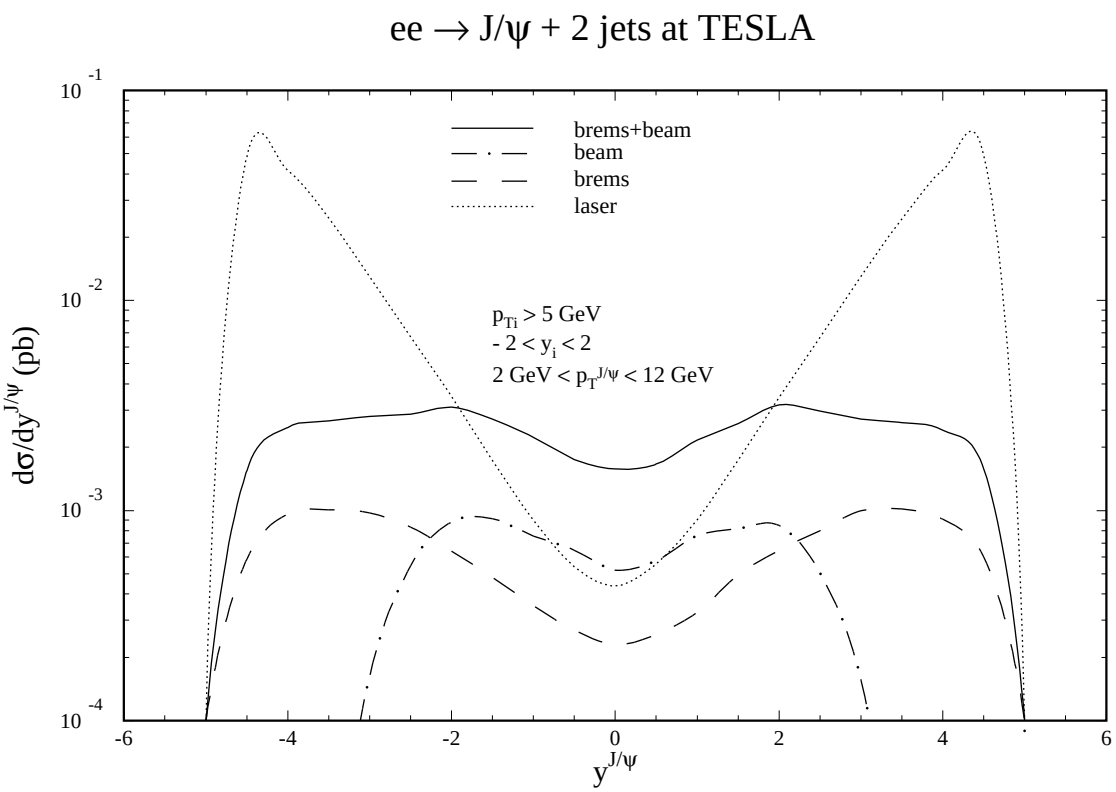

Figure 12: Rapidity distribution $d\sigma/dy$ of $\gamma\gamma \to J/\psi + jj$ via bremsstrahlung, beamstrahlung, their coherent superposition, and laser back-scattering at TESLA.